

Mixed monolayer of a nucleolipid and a phospholipid has improved properties for spectroelectrochemical sensing of complementary nucleobases

Francisco Prieto Dapena^{a*}, ZhangFei Su^b, Julia Alvarez Malmagro^{a,b}, Manuela Rueda^{a*}, Jacek Lipkowski^{b*}

^a Department of Physical Chemistry, University of Seville, C/Professor García González nº 2, 41012 Seville, Spain.

^b Department of Chemistry, University of Guelph, Guelph, Ontario, Canada N1G 2W1.

Corresponding authors:

Francisco Prieto: dapena@us.es

Manuela Rueda: marueda@us.es

Jacek Lipkowski: jlipkows@uoguelph.ca

In honor of Professor Juan Feliu on the occasion of his 70th birthday and in recognition of his outstanding contributions to electrochemistry

Abstract

A mixed monolayer of 1,2-dipalmitoyl-sn-glycero-3-(cytidine diphosphate) nucleolipid (DG-CDP) and 1,2-dipalmitoyl-sn-glycero-3-phosphocholine (DPPC) was transferred from the air-water interface onto an gold (111) electrode surface using the Langmuir-Schaeffer (horizontal touch) technique. Compression isotherms were recorded for the monolayer spread at the air-water interface. These measurements demonstrated that the mixture composition 7:3 of DG-CDP:DPPC displayed reduced repulsive interactions between polar heads and ideal packing of acyl chains. Chronocoulometric experiments were performed to demonstrate stability of this film at the gold– solution interface. Photon polarization modulation infrared reflection absorption spectroscopy showed that the tilt angle of the acyl chains is slightly higher, and the chains are less twisted in the mixed than in the pure nucleolipid monolayer. In the mixed film, the tilt of the cytosine moiety (the sensing element of the monolayer) assumes a large angle with respect to the surface normal, even when the monolayer becomes detached from the gold surface. The mixed monolayer has improved properties for future applications for detection of guanine, its complementary base.

Keywords: mixed lipid monolayer, 1,2-dipalmitoyl-sn-glycero-3-cytidine nucleolipid, 1,2-dipalmitoyl-sn-glycero-3-phosphocholine, polarization modulation infrared reflection absorption spectroscopy (PM-IRRAS), spectroelectrochemical sensing.

1- Introduction

Investigations of molecular recognitions capabilities of DNA bases located on electrode surfaces can be used for the development of electrochemical biosensors that take advantage of the specificity of Watson-Crick interactions between complementary bases [1]. Moreover, these studies can shed some light on the possible effects of static electric fields of the same order as in biological membranes acting on the nucleobases tautomeric and acid-base equilibria and the intermolecular interactions.

This was the motivation of our studies of DNA bases adsorbed on gold electrodes, using a combination of electrochemical methods, *in situ* scanning tunneling microscopy (STM) and absorption reflection Fourier transform infrared spectroscopy (FT-IRRAS) [2–8]. These studies concluded that the interactions of the bases with the electrode surface modify the tautomeric equilibria and the interactions between complementary bases adsorbed on the bare gold electrode are not involving the specific Watson-Crick hydrogen bonds formation.

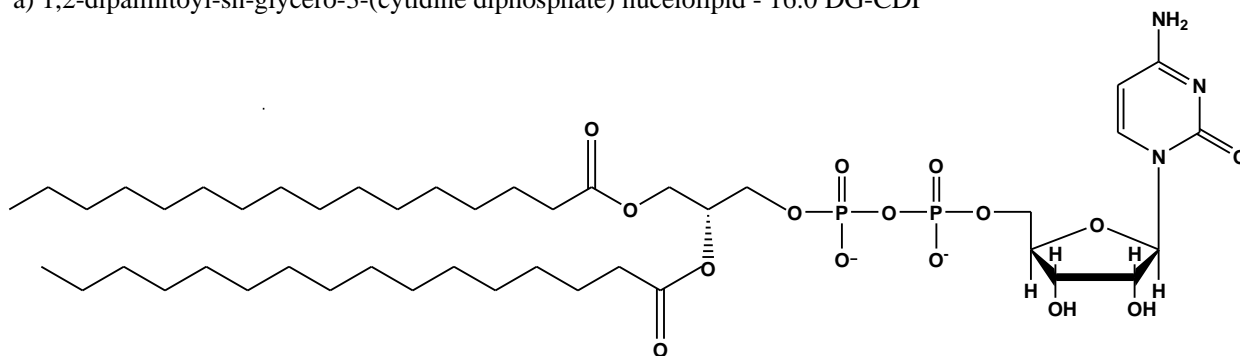
To overcome this problems, we deposited monolayers of 1,2-dipalmitoyl-sn-glycero-3-(cytidine diphosphate) nucleolipid (16:0 DG-CDP) (Figure 1) on bare gold electrodes, by transferring Langmuir monolayers prepared at the air/water interface to the electrode surface by the Langmuir-Shafer method (horizontal touch). The molecules forming the monolayer were then oriented with the hydrophobic tails towards the electrode surface, while the polar head containing the nucleobase derivative towards the electrolyte, preventing their interaction with the electrode surface [9]. The characterization of these modified electrodes by differential capacity and charge density measurements allowed us to determine the stability of the system as a function of the electrode potential. Moreover, photon polarization modulation infrared reflection

absorption spectroscopy (PM-IRRAS) showed that acyl chains of the lipids were in the gel state. They also provided information concerning the orientation of the cytosine moiety of the nucleolipid and its reorientation caused by a change of the electrode potential.

Several studies with nucleolipid monolayers formed at the air water interphase demonstrated molecular recognition capabilities of these monolayers to the complementary DNA bases [10–17]. Our work with 16:0 DG-CDP monolayers on gold electrodes, previously incubated with guanine in 0.1 M NaF solutions, showed the existence of specific Watson-Crick interactions between the cytosine moiety of the nucleolipid and guanine at positive electrode charge densities and non-specific interactions at negatively charged surfaces [18]. This knowledge could be used for the preparation of functionalized liposomes for drug delivery.

The main contribution to the stability of the nucleolipid monolayer must be the lateral hydrophobic interactions between adjacent acyl chains. However, the Langmuir isotherms for 16:0 DG-CDP and for 1,2-dipalmitoyl-sn-glycero-3-phosphocholine (DPPC) (Figure 2), both with identical hydrophobic tails, show that the maximum area per molecule in the 16:0 DG-CDP monolayer (c.a. 60 \AA^2) is higher than in the DPPC monolayer (c.a. 40 \AA^2). This difference indicates the existence of either repulsive and/or steric interactions between the polar heads of the nucleolipid molecules, originating in a less densely packed monolayer than the monolayer of DPPC.

a) 1,2-dipalmitoyl-sn-glycero-3-(cytidine diphosphate) nucleolipid - 16:0 DG-CDP



b) 1,2-dipalmitoyl-sn-glycero-3-phosphocholine (DPPC)

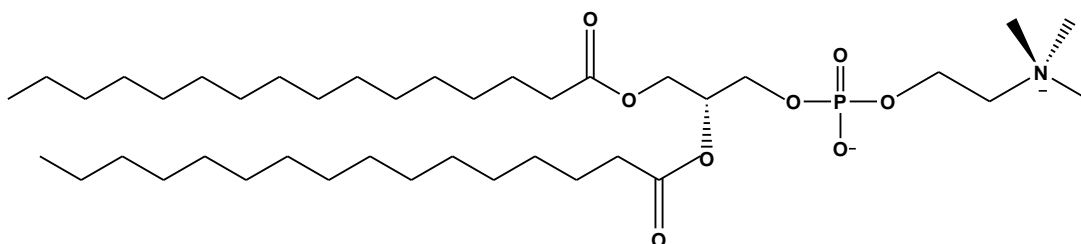


Figure 1. Molecular structure of a) 1,2-dipalmitoyl-sn-glycero-3-cytidine diphosphate (DG-CDP) and b) 1,2-dipalmitoyl-sn-glycero-3-phosphocholine (DPPC)

The objective of this work is to prepare and characterize monolayers supported on a gold (111) electrode containing a mixture of 16:0 DG-CDP and DPPC, in order to obtain lower molecular areas at high surface pressures, thus maximizing the acyl chain lateral interactions, and to increase the separation between polar heads that may facilitate the host-guest interactions between cytosine moiety of the nucleolipid and guanine. These films should be more suitable for the future development of nucleic acid- based biosensors and liposomes for drug delivery with molecular recognition capabilities.

2- Experimental

2.1- Reagents, solutions and electrodes.

The 1 mg mL⁻¹ stock solutions of 1,2-dipalmitoyl-sn-glycero-3-cytidine purchased from Avanti Polar Lipid, were prepared in chloroform and stored at -20 °C. Solutions of mixtures of both lipids with the desired final molar fractions were prepared by mixing the stock solutions of the individual lipids to give the desired molar fraction .

Solutions of 0.1 M NaF (Sigma-Aldrich - BioXtra, 99%) prepared from freshly purified ultrapure Milli-Q water were used for electrochemical experiments. Solutions of 0.1M NaF in D₂O (Cambridge Isotope Laboratories) were employed in PM-IRRAS measurements. Solid NaF in the powder form was previously cleaned from organic impurities in an UV ozone chamber (Jelight) for 15 min.

A home-grown gold (111) single crystal and Ag/AgCl (saturated KCl, Pine Research Instrumentation, -0.045 V vs SCE) were employed as the working and the reference electrodes in PM-IRRAS experiments. A Mateck gold (111) single crystal of 0.159 cm² and a Hg/Hg₂SO₄ (saturated K₂SO₄, Radiometer, +0.400 V vs SCE) were used as the working and reference electrodes in the electrochemical measurements. The gold (111) single crystal electrodes were cleaned by flame annealing in a blue gas torch and cooled in air, before every experiment. A flame-annealed gold wire was employed as the auxiliary electrode in the electrochemical measurements and a platinum foil in PM-IRRAS experiments. All the measurements were performed at room temperature (22 ± 2 °C). All potentials are reported versus the saturated calomel electrode (SCE) by converting the measured potentials into the SCE scale.

The glassware was cleaned by immersion in a potassium permanganate bath overnight. The residuals of MnO₂ were eliminated with a diluted piranha mixture (3:1 H₂SO₄/H₂O₂ v/v) in ultrapure water. Following that, the glassware was meticulously rinsed with copious amount of Milli-Q water. PTFE components of the spectroelectrochemical cell were cleaned in the piranha solution and thoroughly rinsed with Milli-Q water.

2.2- Preparation of the monolayers, measurements of the Langmuir isotherms and transfer of the monolayers to the gold single crystal (111) electrode.

A 611D Langmuir trough made from PTFE (270 cm² of area and c.a. 150 cm³ of subphase volume) was used for the measurement of Langmuir isotherms. The trough is equipped with two PTFE moving barriers and a PS4 Nima pressure sensor. A new strip of 1 cm wide Whatman[®] chromatographic paper was used as the Whilhelmy plate in every measurement. The trough was cleaned with methanol and rinsed with Milli Q water before every measurement. The trough was placed in a cabinet to prevent contaminations and disturbance of the pressure sensor by streams of air.

The monolayers were prepared by spreading a volume of 20-30 μL of lipids solution over the air/water interphase in the Langmuir trough with open barriers. The solvent of the lipid solution was allowed to evaporate for a period of 20 min. Then, the barriers compressed the monolayer at a rate of $25 \text{ cm}^2/\text{min}$, while the surface pressure was registered.

The Langmuir-Shaefer method was used to transfer the monolayers onto the gold single crystal (111) electrode at the equilibrium pressure, 30 mN m^{-1} . The equilibrium spreading pressure was determined in an independent experiment. The electrode was previously flame annealed and cooled over the monolayer in the Langmuir trough for 30 min. By means of a step motor, the electrode was brought horizontally to contact the monolayer and was withdrawn. It was then allowed to dry in the Ar atmosphere of the electrochemical cell for 60 min.

Electrochemical and PM-IIRAS instrumentation and measurements has been described thoughtfully in a previous work. [9]. A detailed description is also included in the supplementary information file.

An Autolab PG-STAT30 from Methrom was used for the electrochemical measurements, that were carried out in a conventional three electrode cell. Solution electrolyte was degassed by bubbling Ar during 30 min before the contact with the working electrode was established. A flow of Ar was maintained over the electrolyte during the whole experiment.

The purity of 0.1 M NaF electrolyte was verified by recording differential capacitance curves (DC) of the gold (111) electrode and comparing them to curves previously reported in the literature [15–17].

The surface charge densities at the gold (111) electrode were measured by integrating current transient registered when potential was stepped from a value at which the monolayer was present at the gold surface to the potential -0.8 V vs SCE at which it was desorbed (detached) from the surface [19,20]. The procedure of these measurements was described in a previous paper [9]. At potential -0.8 V vs SCE , the charge density of gold (111) electrode initially covered by the monolayer of nucleolipid become equal to the charge of the monolayer free gold electrode.

2.4- IR spectroscopic measurements.

FT-IR measurements were performed with a Nicolet Nexus 8700 (ThermoFisher) spectrometer equipped with a MCT-A detector cooled with liquid nitrogen and controlled by the Omnic software. An external tabletop optical mount (TOM) box was used, equipped with the MCT-A detector, the sample compartment and the optical head (II/ZS50 ZnSe 50 kHz) of the photoelastic modulator (PEM, PM-90 from Hinds Instruments). The sampling demodulator (GWC Instruments Synchronous Sampling Demodulator), was used for PM-IRRAS measurements. A CaF₂ equilateral prism (Boxin Photoelectronic Co.) freshly cleaned with methanol, with Milli-Q water and in the Ozone UV chamber during 10 min., was the IR window in the spectroelectrochemical cell. The electrode potential was applied with a HEKA PG590 potentiostat, controlled by an Omnic macro that triggered the potential changes and the spectra collection.

The gold (111) electrode modified with the nucleolipid monolayer was transferred to the spectroelectrochemical cell containing 0.1 M NaF in D₂O. The oxygen from the electrolyte solution was removed by bubbling argon during 20 min and then the electrode was pressed against one side of the CaF₂ prism. The spectrometer and the TOM box were purged several hours before the collection of the spectra and during the whole experiment with dry and CO₂ free air using purge gas generator (Parker Blaston). The electrode potential was changed from 0.35 V vs SCE to -0.84 V vs SCE in steps of -0.1 V. The chronocoulometric experiments were performed up to potential -0.8 V vs SCE. Figure S 1 of the supporting information shows that capacitance of the interface is similar for the bare gold electrode and electrode initially covered by the mixed monolayer for more negative potentials. However, it is now well documented that when the monolayer is detached from the electrode surface it remains in the proximity of the electrode separated by ~ 1nm thick layer of the electrolyte. The potential drop across the interface takes place between the gold surface and the thin layer of electrolyte below the film and hence the presence of the film is no longer probed by chronocoulometry or differential capacitance. In contrast, it is detected by PM IRRAS. For this reason, the PMIRRAS measurements were performed to potentials up to - -0.845 V vs SCE.

The IR spectra at each potential were generated by averaging 4000 scans to provide an adequate signal to noise ratio with an instrument resolution of 4 cm⁻¹. The electrolyte thickness was 1-10 μm. It was determined at each experiment by the procedure described in ref [21]. Independent measurements were performed for different spectral regions of interest (C-H stretching regions around 3000 cm⁻¹ and C=O, C=C and C=N stretching

region around 1600 cm⁻¹). The incidence angle of the IR beam and the half-wave retardation of the photoelastic modulator were selected to optimize the enhancement of the mean square electric field strength (MSEFS) of the polarized radiation at the electrode surface. The procedure of PM-IRRAS measurements and signal processing has been described in detail in previous studies [21,22].

After correction for the PEM response functions, the PM-IRRA spectra plot ΔS vs wavenumber, with ΔS being proportional to the surface concentration of the adsorbed species, Γ and defined as:

$$\Delta S = \frac{R_p - R_s}{R_p + R_s} = 2.3 \varepsilon \Gamma \quad (1)$$

R_p and R_s are the reflectance with p and s radiation, respectively, and ε is the molar absorption coefficient of the adsorbed species.

To allow quantitative analysis of the PM-IRRAS data, the spectra of the mixed monolayers with randomly oriented molecules were simulated by solving the Fresnel equations for four parallel homogeneous phases (CaF₂|D₂O|DPPC or 16:0 DG-CDP|Au) by the transfer matrix method. The optical constants of the lipidic phase were obtained from the transmission spectra and its thickness was considered 3 nm, a half of the thickness of a DPPC bilayer. [23] The optical constants used in these calculations are given in Figures SI 1 a and b. The optical constants for D₂O, Au, and CaF₂ were taken from the literature [24–26].

3- Results and discussion.

3.1- Langmuir isotherms of mixed DG-CDP:DPPC monolayers

The compression isotherms at the air-solution interface have been recorded in order to describe packing of lipids in mixed DG-CDP:DPPC monolayers. Figure 2a presents compression isotherms of mixed DG-CDP:DPPC monolayers with different molar fractions of the nucleolipid (DG-CDP).

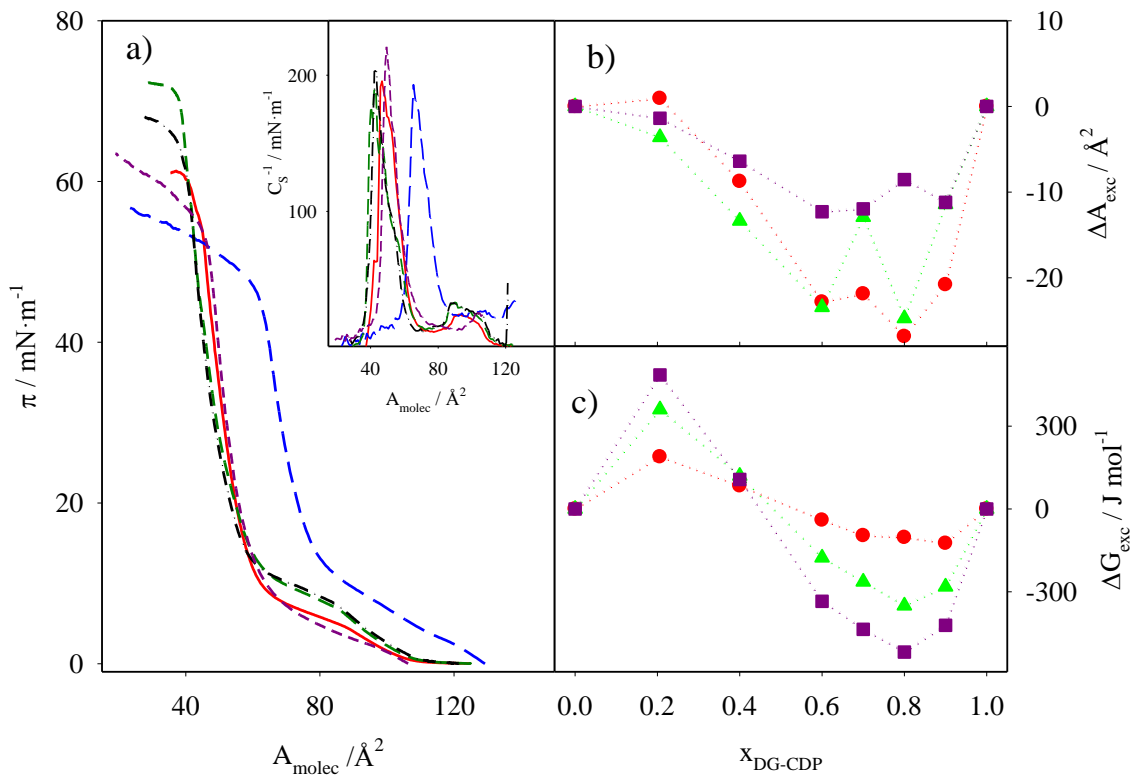


Figure 2. a) Compression isotherms determined at 22°C for the mixed DG-CDP:DPPC monolayers with molar fractions of DG-CDP ($x_{\text{DG-CDP}}$): $x_{\text{DG-CDP}}=0$ (red solid line), $x_{\text{DG-CDP}}=1$ (blue dashed line), $x_{\text{DG-CDP}}=0.2$ (green dashed line), $x_{\text{DG-CDP}}=0.4$ (black dot-dash line) and $x_{\text{DG-CDP}}=0.7$ (pink dashed line), measured at pure water subphase. Inset plots compression modulus, C_s^{-1} , defined as $C_s^{-1} = -A_{\text{molec}}(d\pi/dA_{\text{molec}})$ versus the area per molecule; b) mean molecular excess area and c) excess Gibbs free energy plotted as a function of the mol fraction of DG-CDP at surface pressures of 5 mN m⁻¹ (red circles), 15 mN m⁻¹ (green triangles) and 30 mN m⁻¹ (blue squares).

Figure 2a shows that the presence of DPPC in the monolayer, causes a decrease of the mean molecular area at the collapse pressure up to values very close to those of the pure DPPC film (close to 40 Å²) as compared to the values obtained for the pure nucleolipid monolayer, c.a 60 Å². To examine this effect in further details, inset to Figure 2a plots the compression modulus calculated from these isotherms. For all monolayers the compression modulus is approaching 175 mN m⁻¹ when film pressures are higher than 10 mN m⁻¹, indicating that at these conditions the films are in the gel state. Figure 2b plots, the excess molecular area calculated using the equation:

$$\Delta A_{exc} = A_{molec} - (x_{DG-CDP} \cdot A_{(x_{DG-CDP}=0)} + (1 - x_{DG-CDP}) \cdot A_{(x_{DG-CDP}=1)}) \quad (2)$$

as a function of the mole fraction of the nucleolipid (x_{DG-CDP}).

For $x_{DG-CDP} > 0.2$ the ΔA_{exc} values are negative indicating better packing of the molecules. Figure 2c shows changes of the excess Gibbs energy of the film calculated from:

$$\Delta G_{exc} = \int_0^{\pi} \Delta A_{exc} d\pi \quad (3)$$

as a function of the mole fraction of nucleolipid. The ΔG_{exc} values are positive at $x_{DG-CDP} < 0.4$ indicating that the interactions between the molecules are repulsive. In contrast, ΔG_{exc} become negative at $x_{DG-CDP} > 0.4$. These values indicate attractive interaction, most likely due to reduced electrostatic repulsion between negatively charged polar heads of the nucleolipid. At 30 mN m^{-1} , the ΔG_{exc} plot (Figure 2c) display a pit for x_{DG-CDP} between 0.6 and 0.9 with ΔG_{exc} values lower than -300 J mol^{-1} indicating a good mixing of the two lipids. The minimum of ΔG_{exc} is observed for $x_{DG-CDP}=0.8$. However, to achieve a better dispersion of the nucleolipid we have decided to perform further studies at performed at the equilibrium spreading pressure and the mixed monolayer with 7:3 molar ratio of DG-CDP:DPPC. At the equilibrium spreading pressure of the film with 7:3 molar ratio of DG-CDP:DPPC (30 mNm^{-1}), $\Delta A_{exc} = -10 \text{ \AA}^2$ and $\Delta G_{ex} = -400 \text{ J mol}^{-1}$. These numbers indicate somewhat better packing of molecules than in the pure monolayer of the nucleolipid and reduced electrostatic interactions between the polar heads.

3.2- Surface charge density.

The charge density curve (σ vs E) for the gold (111) electrode covered by the mixed monolayer of DG-CDP:DPPC with 7:3 molar ratio is showed in Figure 3. For comparison the curves for the film free gold electrode and the electrode covered by the monolayer of pure nucleolipid are also shown in this figure. The potential of zero charge, E_{pzc} , given by the intersection of the charge density plot with the zero-charge density line, corresponds to -0.4 V vs SCE for electrode with the mixed monolayer and is about 0.6 V vs SCE more negative than E_{pzc} of the film free electrode. Since the nucleolipid is negatively charged such large shift is expected [27]. Significantly, this value is more negative than for the pure nucleolipid monolayer covered gold electrode. This fact is

consistent with lower surface concentration of the negatively charged nucleolipid in the film of pure nucleolipid. The charge densities for the electrode covered by pure monolayer transferred at room temperature are higher than reported previously for the monolayer transferred at 44 °C [9]. At room temperature the monolayer is in the gel state and at 30 mN m⁻¹ the mean molecular area in the film corresponds to ~65 Å². In contrast at 44 °C the monolayer is in the liquid expanded state and the corresponding mean molecular area is ~80 Å². This translates to significantly higher density of negatively charge lipids in the monolayer transferred at room temperature. In general, the charge density curves show that the mixed monolayer is stable at the gold surface in the range of potentials between +0.3 and -0.4 V vs SCE. A detachment (electrodewetting) of the film takes place at more negative potentials, as can be observed in figure SI 1, that shows differential capacitance plots. The monolayer is totally detached (desorbed) from the electrode surface at E < -0.75 V vs SCE.

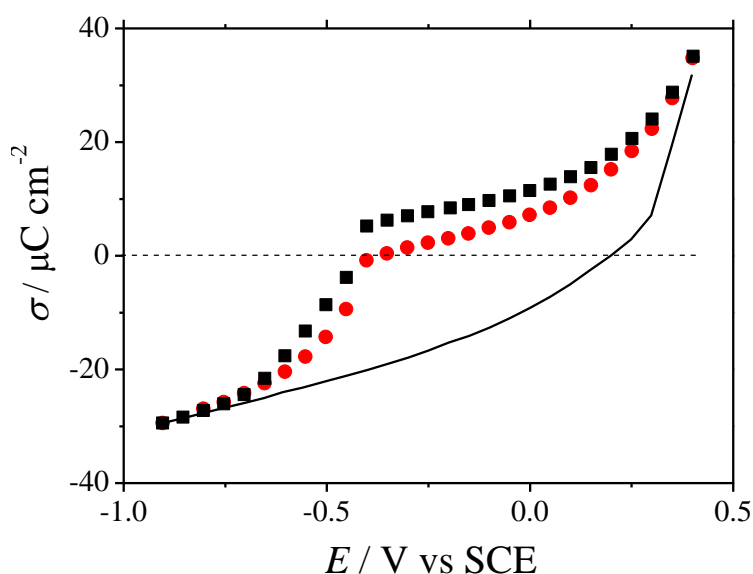


Figure 3. Charge density versus potential plots obtained for gold (111) electrodes in 0.1 M NaF solutions: covered with a mixed DG-CDP:DPPC monolayer in a molar ratio 7:3 (red circles) and covered with a pure nucleolipid monolayer (black squares) and a monolayer free gold (111) electrode (solid line).

3.3- PM-IRRAS studies

3.3.1- PM-IRRAS spectra in the C-H stretching region

The PM IRRAS experiments were performed in D₂O. The isotope exchange does not take place in the acyl chains of the lipids. Hence, the lateral interactions between acyl chains are not affected when D₂O is used as the solvent. D₂O may have minor effect on hydration of the polar head groups which may lead to small shift of position of the corresponding bands. However, the differences between properties of the monolayer in H₂O and D₂O are minor. Figure 4 shows the C-H stretching spectra of the mixed monolayer recorded at several potentials in the range from 0.36 to -0.84 V vs SCE.

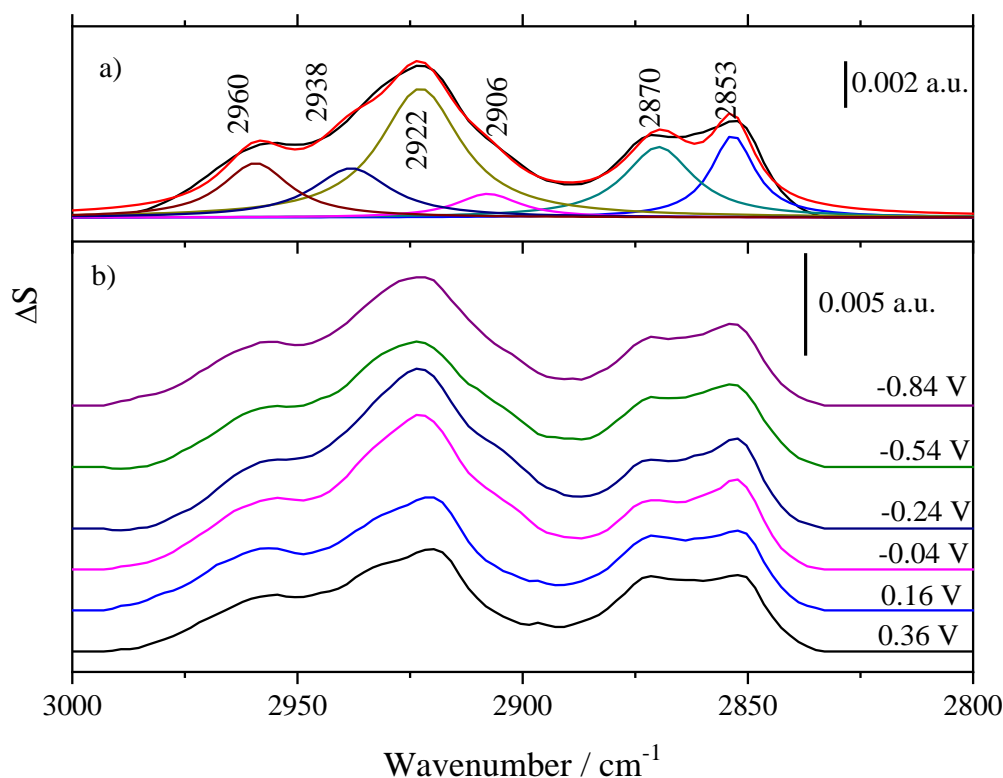


Figure 4. PM-IRRAS spectra of the mixed DG-CDP:DPPC (7:3) monolayer on the gold (111) electrode: a) Averaged spectrum in the potential range from 0.36 to -0.84 V vs SCE experimental (black solid line) and b) Single spectra at the indicated potentials. The monolayer was transferred from the air-water interface at surface pressure 30 mNm⁻¹ using the LS technique.

The PM-IRRAS spectra in Figure 4 show broad bands that can be deconvoluted into individual sub-bands, as shown in Fig. 4a. The deconvolution of the averaged spectrum provides four normal coordinate bands at $2853 \pm 1 \text{ cm}^{-1}$ ($\nu_s(\text{CH}_2)$), $2870 \pm 1 \text{ cm}^{-1}$ ($\nu_s(\text{CH}_3)$), $2922 \pm 1 \text{ cm}^{-1}$ ($\nu_{as}(\text{CH}_2)$) and $2960 \pm 1 \text{ cm}^{-1}$ ($\nu_{as}(\text{CH}_3)$). In addition, two small bands at $2906 \pm 1 \text{ cm}^{-1}$ and $2938 \pm 1 \text{ cm}^{-1}$ could be identified as corresponding to the Fermi resonances [21]. The position and the full width at half-maximum (fwhm) of $\nu_s(\text{CH}_2)$

($2853\pm 1\text{ cm}^{-1}$ and $15\pm 1\text{ cm}^{-1}$) and $\nu_{\text{as}}(\text{CH}_2)$ ($2922\pm 1\text{ cm}^{-1}$ and $21\pm 1\text{ cm}^{-1}$), are very close to the corresponding values in the monolayer of pure DPPC in the gel state [28], and indicate a predominant all-*trans* conformation of the acyl chains [29,30]. The integrated intensity of a single PM-IRRAS band can be used to calculate the orientation of the transition dipole of the corresponding vibration [21]:

$$\cos(\theta)^2 = \frac{1}{3} \frac{A_{\text{exp}}}{A_{\text{theor}}} \quad (4)$$

Where θ is the angle between direction of the transition dipole and the normal to the electrode surface, A_{exp} and A_{theor} are the integrated intensities of the experimental PM-IRRAS band and the band calculated for the monolayer with randomly oriented molecules using optical constants shown in Figure SI 2a of the Supporting Information. Using equation (4) and the integrated intensities of the bands at 2853 cm^{-1} and 2922 cm^{-1} , the angles $\theta_{\nu_s(\text{CH}_2)}$ and $\theta_{\nu_{\text{as}}(\text{CH}_2)}$ corresponding to directions of the transition dipoles of the two methylene bands can be determined. The two transitions dipoles are in the plane of the methylene group and are normal to the axis of the *trans* stretched acyl chain, as shown in Figure 5b. Therefore, the following relation between the tilt angle of the acyl chain relative to the electrode normal, θ_{tilt} , and $\theta_{\nu_s(\text{CH}_2)}$ and $\theta_{\nu_{\text{as}}(\text{CH}_2)}$ [31]:

$$\cos(\theta_{\nu_s(\text{CH}_2)})^2 + \cos(\theta_{\nu_{\text{as}}(\text{CH}_2)})^2 + \cos(\theta_{\text{tilt}})^2 = 1 \quad (5)$$

Equation (5) allows one to calculate the average tilt angle of the *trans* fragments of the acyl chains. Figure 5a plots the averaged tilt angles of *trans* fragments of the acyl chains in the mixed monolayer as a function of the electrode potential. For comparison, the tilt angles for the pure monolayer of the nucleolipid, taken from ref [9], are also included in this figure. For the mixed monolayer, the tilt angles of the chains vary between 32° - 36° and weakly depend on the electrode potential. These values are a few degrees higher than in the pure nucleolipid monolayer [9]. However, the differences are within the experimental errors. At potential values $E < -0.4\text{ V vs SCE}$ the tilt angle of the acyl chain decreases to c.a. 30° independently of the potential. This indicates the electro-dewetting of the monolayer, which remains in proximity of the electrode surface as shown by neutron scattering measurements.[32] In the external reflection configuration, lipidic molecules remain in the thin layer with supramolecular organization driven by their insoluble characteristics, rather than assuming random orientation.

The angles θ_{vs} and θ_{vas} could be used to calculate the twist angle (θ_{twist}) of the trans segments of the chain defined as the angle between the -C-C-C- plane and the plane formed by the chain axis and the surface normal [33,34]. The -C-C-C- plane bisects the methylene groups, the $\nu_s(\text{CH}_2)$ and $\nu_{as}(\text{CH}_2)$ transition dipole moments are perpendicular to one another, and θ_{vs} and θ_{vas} are defined with respect to the surface normal. As a result, the twist angle of the acyl chains may be found by the following expression [33,34]:

$$\theta_{twist} = \tan^{-1} \left(\frac{\cos \theta_{vas}}{\cos \theta_{vs}} \right) \quad (6)$$

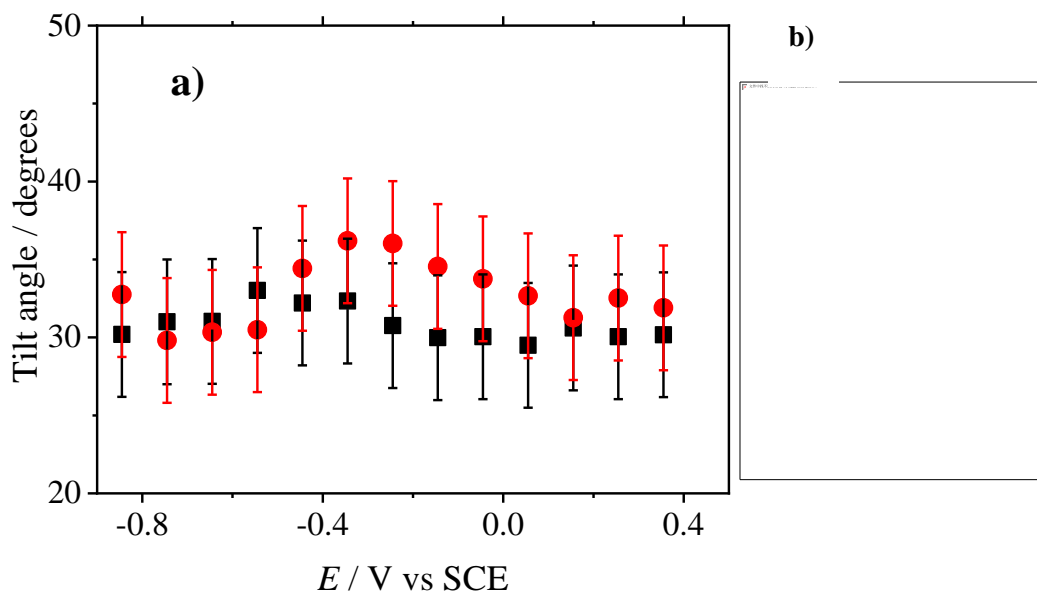


Figure 5. a) Tilt angle of the acyl chains of mixed DG-CDP:DPPC (red circles) and pure DG-CDP (black squares) monolayers supported on gold (111) electrode, as a function of the potential. b) Schematic representation of the tilt angle of the acyl chain and the directions of the transition dipoles corresponding to the vibrational symmetric and antisymmetric stretching modes of methylene groups.

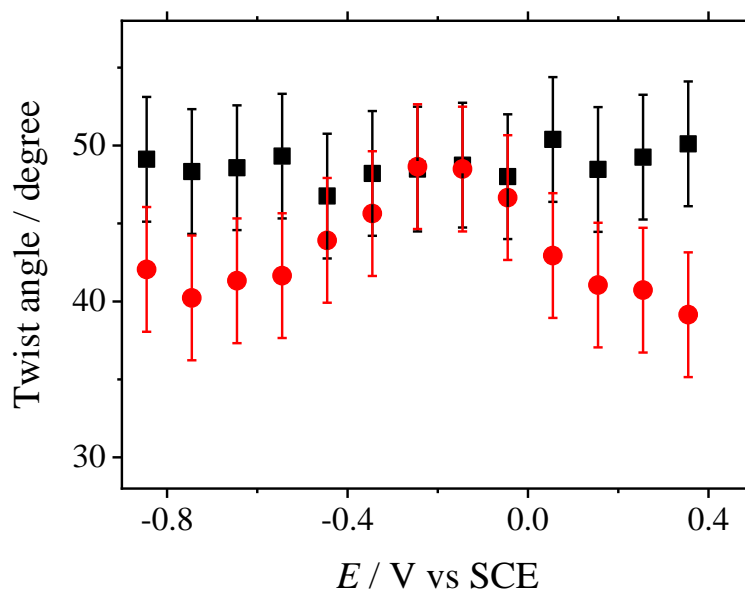


Figure 6. Twist angle of the acyl chains in the DG-CDP:DPPC monolayer (red circles) and DG-CDP monolayer (black squares) on gold (111) surface in 0.1 M NaF as a function of applied potential.

Figure 6 plots twist angles calculated for the mixed and the pure nucleolipid monolayers. The twist angles are between 40° and 45° for the mixed monolayer and ~50° for the pure monolayer. The changes with the electrode potential are within limits of the experimental errors. A twist angle of 45° is referred to as the trivial twist angle and corresponds to no preferential acyl chain twisting [33,34]. Within experimental uncertainties, the twist angles for the mixed monolayer are equal to the trivial twist angle, indicating that the acyl chains are not twisted. The twist angles for the pure monolayer are ~5° higher than the trivial twist angle indicating that the chains are slightly twisted in this monolayer.

3.3.2- PM-IRRA spectra of the head group

Figure 7a shows the potential averaged spectrum of the mixed DG-CDP:DPPC monolayer on the gold (111) electrode, in the spectral region from 1800 to 1400 cm^{-1} . The positions of the absorption bands are almost identical to the position in the PM-IRRA spectrum of pure nucleolipid monolayer [9], and very close to the positions in the spectrum (Figure SI 3 of the Supporting Information) calculated from the optical constants obtained from the transmission spectra of vesicles. Therefore, the following

band assignment can be made: the bands at 1740 and 1726 cm^{-1} correspond to the non-hydrogen bonded and hydrogen bonded C=O stretching of the glycerol fragment. The spectrum corresponding to pure DPPC vesicles shows only the non-hydrogen bonded glycerol C=O band. The presence of both non-hydrogen bonded and hydrogen bonded bands in spectrum of the mixed monolayer indicates that the polar head group of the nucleolipid favors the hydrogen bond formation with the glycerol moiety, as compared to the choline group.

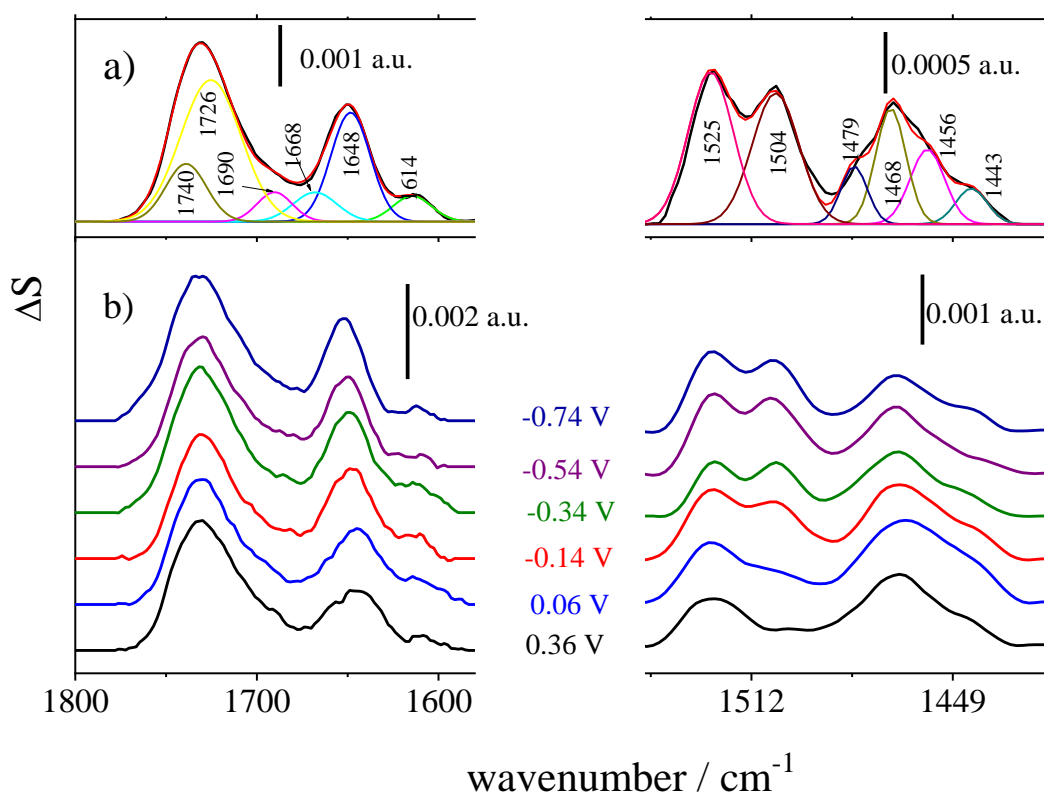


Figure 7. 1800- 1400 cm^{-1} PM-IRR spectra of the mixed DG-CDP:DPPC monolayer on the gold (111) electrode: a) Averaged spectrum in the potential range from 0.36 to -0.84 V vs SCE experimental (black solid line) and b) Single spectra at the indicated potentials. The monolayer was transferred from the air-water interface at surface pressure 30 mNm^{-1} using the LS technique.

The absorption bands at 1614 cm^{-1} and 1648 cm^{-1} correspond to bands at 1604 and 1643 cm^{-1} present in the transmission IR spectrum of the canonical tautomer cytosine in neutral D_2O solutions [8], assigned to the stretching modes of $\text{C5}=\text{C6}$ and $\text{C}=\text{O}$, respectively. The

small bands at 1690 cm^{-1} and 1668 cm^{-1} are not present in the transmission IR spectrum of cytosine in D_2O neutral solutions [8]. Figure SI 4 of the supporting information shows the comparison of the experimental PM IRRAS and simulated spectra calculated from vesicles measured in transmission and second derivative of these bands. However, at low pH values, at which cytosine is protonated, two absorption bands can be observed at 1670 cm^{-1} and at c.a. 1700 cm^{-1} . The presence of the bands at 1668 and 1690 cm^{-1} , both in the PM-IRRAS spectrum of the supported monolayer and in the transmission IR spectrum of nucleolipid vesicles in neutral D_2O solutions suggest that cytosine moiety is strongly hydrated, assisted by the presence of hydrated cations attracted to the negatively charged polar head of the nucleolipid.

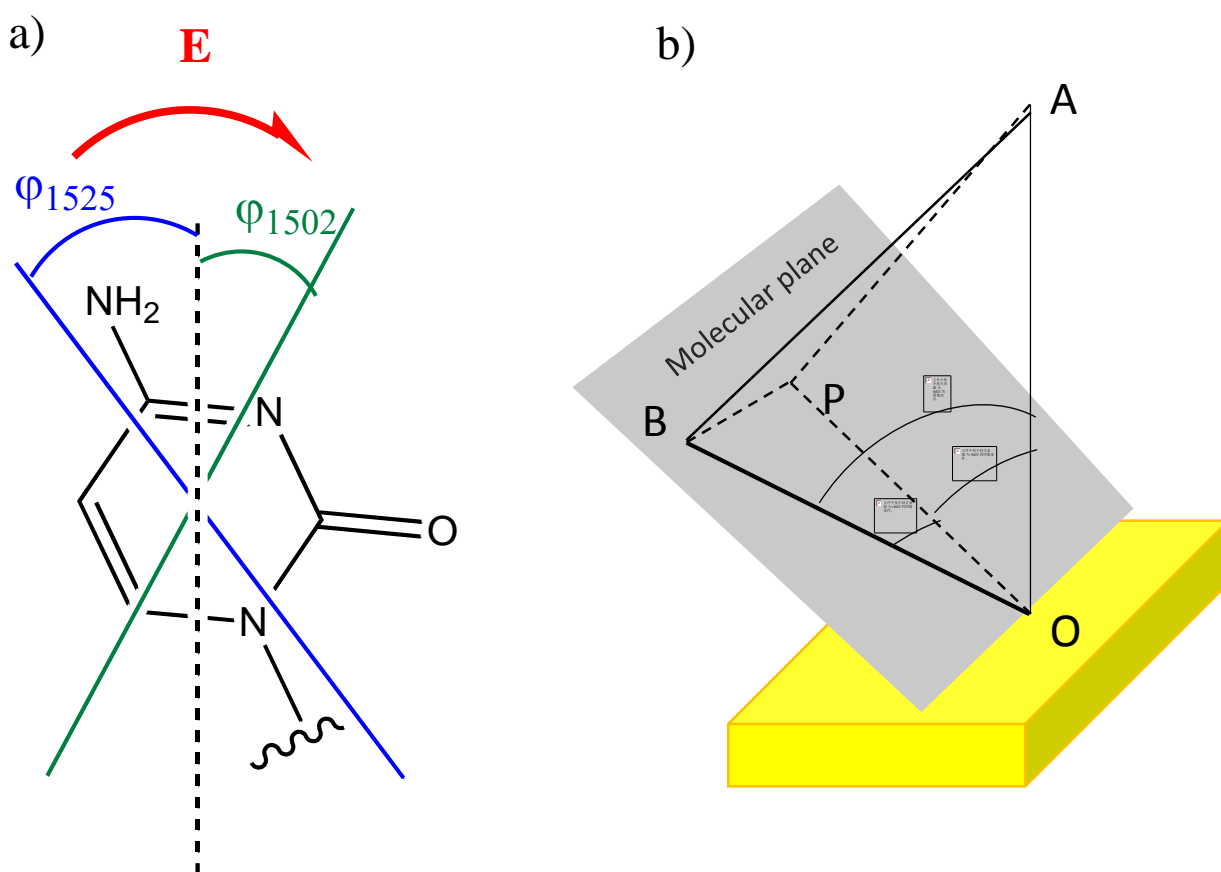


Figure 8. - a) Schematic frontal view of the cytosine moiety molecular plane including the directions of the transition vectors of the vibrations at 1525 cm^{-1} (blue) and 1502 cm^{-1} (green). Black dashed line represents the projection of the normal direction to the electrode surface over the molecular plane and the red curved arrow indicate the clockwise rotation of the molecular plane as the potential increases. b) Schematic representation of the molecular plane and the directions normal to the electrode surface

(\overline{OA}) , projected normal to the molecular plane (\overline{OP}), projected normal to the surface onto the molecular plane (\overline{AP}), direction of the transition dipole moment of a given vibration mode (\overline{OB}) and direction in the molecular plane parallel to the electrode surface. (\overline{BP}).
Reprinted from [9] with permission

The bands at 1525 and 1504 cm^{-1} , correspond to the stretching vibrational modes C4N7 and C4C5 of cytosine moiety, respectively [9]. The absorption bands between 1500 and 1400 cm^{-1} correspond to the sugar fragment of the nucleolipid. The integrated

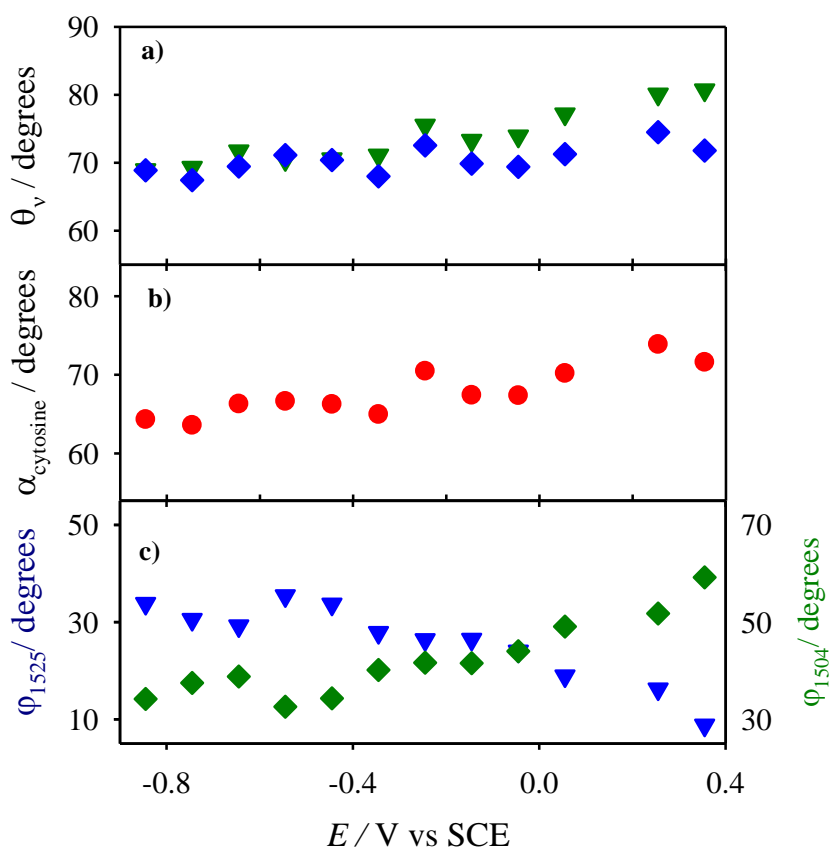


Figure 9. Potential dependence of: a) tilt angles corresponding to the vibrations at 1504 cm^{-1} (green triangles) and 1525 cm^{-1} (blue diamonds) of a mixed DG-CDP:DPPC monolayer. b) Tilt angles of the cytosine moiety molecular plane relative to the surface normal and c) rotation angles of the tensors corresponding to the vibrations at 1504 cm^{-1} and 1525 cm^{-1} relative to the projected direction of the surface normal over the cytosine moiety plane.

intensities of the deconvoluted bands and Equation (4) provide information about angles θ between the direction of transition dipole of a given vibration and the normal direction to the electrode surface. The bands at 1504 and 1525 cm^{-1} have transition dipoles located within the molecular plane of cytosine moiety, which directions determined by DFT

calculations are shown in Figure 8a [8]. The values of θ_{1504} and θ_{1525} are plotted in Figure 9a. Using the procedure described in ref [9] they could be used to calculate the angle between the surface normal and its projection on the surface of cytosine moiety, α , which is a measure of the tilt of the cytosine moiety. They also allow one to calculate angles φ_{1504} and φ_{1525} , which show rotation of cytosine moiety with respect to projection of the surface normal on the moiety plane. Figure 8b shows the definition of angles α , φ_{1504} and φ_{1525} .

Figure 9b show changes of the tilt angle α with the electrode potential. The tilt angles vary between 70° and 65° indicating that the cytosine moiety assumes orientation between 20° and 25° with respect to the plane of the monolayer. These small values indicate that it is nearly parallel to the monolayer surface. The changes with potential are small. Figure 9c plots changes of angles φ_{1504} and φ_{1525} as a function of the electrode potential. In contrast to small changes of the tilt angle α , changes of angles φ_{1504} and φ_{1525} amount to about 20° between positive and negative ends of potentials. These changes are significant and indicate that the plane of the cytosine moiety rotates when potential is changing. Figure SI 5 of SI shows a comparison of the potential dependence of angles φ_{1504} and φ_{1525} on the electrode potential for the mixed and the pure nucleolipid monolayers. Similar rotation of angles φ_{1504} and φ_{1525} is observed for the two monolayers

Figure 10 compares tilt angles of cytosine moiety in the mixed and pure nucleolipid monolayers. In contrast to small differences between rotation angles φ_{1504} and φ_{1525} the differences between tilt angles of the cytosine moiety in the pure nucleolipid and the mixed monolayers are notable. At potentials more positive than -0.2V vs SCE the tilt angles in the two monolayers are comparable. However, at more negative potentials the tilt of the cytosine moiety decreases significantly in the pure nucleolipid monolayer. In contrast, the changes are very small in the mixed monolayer. This behavior indicates that structure of the mixed monolayer changes little with the electrode potential even when it becomes detached from the metal surface at $E < -0.4\text{V}$ vs SCE.

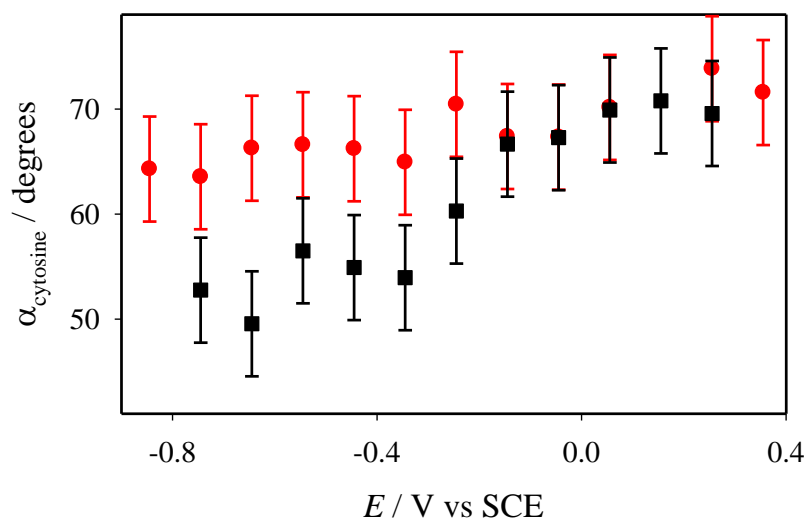


Figure 10. Potential dependence of tilt angles of the cytosine moiety molecular plane relative to the normal direction to the electrode surface for a mixed monolayer (red circle) and a pure nucleolipid monolayer (black squares) transferred at gold (111) electrode at 30 mN m^{-1} from the air/water interphase.

4- Summary and Conclusions

Our goal was to improve stability of a monolayer of a nucleolipid with cytosine in the polar head group, deposited onto a gold electrode surface [9]. It served for detection of guanine, its complementary base [17]. Cytidine diphosphate, the polar head group of the nucleolipid, is a dianion. Therefore, significant electrostatic repulsions between the polar heads of the lipids were present in the monolayer. To minimize the electrostatic effects, we have dispersed the nucleolipid by mixing it with DPPC, a phospholipid with the same length of the acyl chains. Compression isotherm measurements of the mixed monolayers, performed at the air-water interface, demonstrated energetically favorable mixing and minimized electrostatic repulsion of the nucleolipid and DPPC at the DG-CDP:DPPC composition 7:3. The chronocoulometric experiments showed that this monolayer displays higher packing of the alkyl chains when transferred onto the gold electrode surface. The PM IRRAS studies revealed that the tilt angle of the acyl chains is only slightly higher, and the chains are less twisted in the mixed than in the pure nucleolipid monolayer. In the mixed film, the tilt of the cytosine moiety (the sensing element of the monolayer) assumes a large angle with respect to the surface normal, even when the monolayer becomes detached from the gold surface. This is a much-desired property which indicated that the sensing ability of the monolayer will not change when the

electrode is affected by unintended negative polarization. In contrast, in the pure monolayer the tilt of the cytosine moiety changes significantly at negative polarization. These properties suggest that the mixed monolayer is a preferred architecture for the development of a guanine sensor, which will be explored in a next work. Although the present studies were performed on an ideal Au(111) electrode. These results could be used to understand the molecular recognition reaction at biosensor build from a polycrystalline electrode.

Acknowledgements

F.P. acknowledges Spain Ministry of Science and Innovation (CTQ2014-57515-C2-1-R and RED2018-102412-T) and Junta de Andalucía (PAI FQM202). J.L. acknowledges a grant from Natural Sciences and Engineering Research Council of Canada (NSERC) (RG-03958).

References

- [1] J.D. Watson, F.H.C. Crick, Molecular Structure of Nucleic Acids: A Structure for Deoxyribose Nucleic Acid, *Nature*. 171 (1953) 737–738. doi:10.1038/171737a0.
- [2] C. Vaz-Domínguez, M. Escudero-Escribano, A. Cuesta, F. Prieto-Dapena, C. Cerrillos, M. Rueda, Electrochemical STM study of the adsorption of adenine on Au(111) electrodes, *Electrochem. Commun.* 35 (2013) 61–64. doi:10.1016/j.elecom.2013.07.045.
- [3] J. Álvarez-Malmagro, F. Prieto, M. Rueda, A. Rodes, In situ Fourier transform infrared reflection absorption spectroscopy study of adenine adsorption on gold electrodes in basic media, *Electrochim. Acta.* 140 (2014) 476–481. doi:10.1016/j.electacta.2014.03.074.
- [4] F. Prieto, J. Alvarez-Malmagro, M. Rueda, J.M. Orts, Tautomerism of adsorbed Thymine on gold electrodes: an in situ surface-enhanced infrared spectroscopy study, *Electrochim. Acta.* 201 (2016) 300–310. doi:10.1016/j.electacta.2015.11.109.
- [5] F. Prieto, Z. Su, J.J.J. Leitch, M. Rueda, J. Lipkowski, Quantitative Subtractively Normalized Interfacial Fourier Transform Infrared Reflection Spectroscopy Study of the Adsorption of Adenine on Au(111) Electrodes, *Langmuir.* 32 (2016) 3827–3835. doi:10.1021/acs.langmuir.6b00635.
- [6] J. Alvarez-Malmagro, M. Rueda, F. Prieto, In situ surface-enhanced infrared spectroscopy study of adenine-thymine co-adsorption on gold electrodes as a function of the pH, *J. Electroanal. Chem.* 819 (2018) 417–427. doi:doi.org/10.1016/j.jelechem.2017.11.054.
- [7] F. Prieto, M. Rueda, J. Álvarez-Malmagro, Electrochemical Impedance Spectroscopy analysis of an adsorption process with a coupled preceding chemical step, *Electrochim. Acta.* 232 (2017) 164–173. doi:10.1016/j.electacta.2017.02.106.
- [8] J. Alvarez-Malmagro, F. Prieto, M. Rueda, In Situ Surface Enhanced Infrared Absorption Spectroscopy Study of the Adsorption of Cytosine on Gold

- Electrodes, *J. Electroanal. Chem.* 849 (2019) 113362.
doi:10.1016/J.JELECHEM.2019.113362.
- [9] J. Alvarez-Malmagro, Z. Su, J. Jay Leitch, F. Prieto, M. Rueda, J. Lipkowski, Spectroelectrochemical Characterization of 1,2-Dipalmitoyl- sn-glycero-3-cytidine Diphosphate Nucleolipid Monolayer Supported on Gold (111) Electrode, *Langmuir*. 35 (2019) 901–910. doi:10.1021/acs.langmuir.8b03674.
- [10] W. Miao, X. Luo, Y. Liang, Molecular recognition of 7-(2-octadecyloxycarbonylethyl)guanine to cytidine at the air/water interface and LB film studied by Fourier transform infrared spectroscopy, *Spectrochim. Acta - Part A Mol. Biomol. Spectrosc.* 59 (2003) 1045–1050. doi:10.1016/S1386-1425(02)00292-5.
- [11] W. Miao, X. Du, Y. Liang, Molecular recognition of nucleolipid monolayers of 1-(2-octadecyloxycarbonylethyl)cytosine to guanosine at the air-water interface and Langmuir-Blodgett films, *Langmuir*. 19 (2003) 5389–5396.
doi:10.1021/la0345690.
- [12] W. Miao, X. Luo, S. Wu, Y. Liang, Fourier transform infrared spectroscopy study on order-disorder transition in Langmuir-Blodgett films of 7-(2-octadecyloxycarbonylethyl)guanine before and after recognition to cytidine, *Spectrochim. Acta - Part A Mol. Biomol. Spectrosc.* 60 (2004) 413–416.
doi:10.1016/S1386-1425(03)00240-3.
- [13] Y. Wang, X. Du, W. Miao, Y. Liang, Molecular recognition of cytosine- and guanine-functionalized nucleolipids in the mixed monolayers at the air-water interface and Langmuir-Blodgett films, *J. Phys. Chem. B*. 110 (2006) 4914–4923. doi:10.1021/jp055046z.
- [14] C. Li, J. Huang, Y. Liang, Molecular Recognition Capabilities of a Nucleolipid Adenosine at the Air / Water Interface and Langmuir-Blodgett Films Studied by Molecular Spectroscopy, *Cell*. 3 (2000) 7701–7707.
- [15] L. Čoga, S. Masiero, I. Drevenšek-Olenik, Lamellar versus compact self-assembly of lipoguanosine derivatives in thin surface films, *Colloids Surfaces B Biointerfaces*. 121 (2014) 114–121. doi:10.1016/j.colsurfb.2014.05.038.

- [16] L. Čoga, L. Spindler, S. Masiero, I. Drevenšek-Olenik, Molecular recognition of a lipophilic guanosine derivative in Langmuir films at the air-water interface, *Biochim. Biophys. Acta - Gen. Subj.* 1861 (2017) 1463–1470. doi:10.1016/j.bbagen.2016.11.038.
- [17] P. G. Argudo, E. Muñoz, J.J. Giner-Casares, M.T. Martín-Romero, L. Camacho, Folding of cytosine-based nucleolipid monolayer by guanine recognition at the air-water interface, *J. Colloid Interface Sci.* 537 (2019) 694–703. doi:10.1016/J.JCIS.2018.11.036.
- [18] J. Alvarez-Malmagro, Julia; Su, ZhangFei; Leitch, J. Jay; Prieto, Francisco; Rueda, Manuela; Lipkowski, Electric field driven molecular recognition reactions of Guanine with 1,2-dipalmitoyl-sn-glycero-3-cytidine monolayer deposited on Gold Electrodes, *Langmuir*. submitted (2019).
- [19] J. Richer, Measurement of Physical Adsorption of Neutral Organic Species at Solid Electrodes, *J. Electrochem. Soc.* 133 (1986) 121. doi:10.1149/1.2108505.
- [20] J. Kunze, J. Leitch, A.L. Schwan, R.J. Faragher, R. Naumann, S. Schiller, W. Knoll, J.R. Dutcher, J. Lipkowski, New Method to Measure Packing Densities of Self-Assembled Thiolipid Monolayers, (2006). doi:10.1021/la0535274.
- [21] A.H. Kycia, Z. Su, C.L. Brosseau, J. Lipkowski, In Situ PM-IRRAS Studies of Biomimetic Membranes Supported at Gold Electrode Surfaces, in: John Wiley & Sons (Ed.), *Vib. Spectrosc. Electrified Interfaces*, 2013: pp. 345–417. doi:10.1002/9781118658871.ch11.
- [22] V. Zamlynyy, J. Lipkowski, Quantitative SNIFTIRS and PM IRRAS of Organic Molecules at Electrode Surfaces, in: R.C. Alkire, D.M. Kolb, J. Lipkowski, P. Ross (Eds.), *Adv. Electrochem. Sci. Eng.*, Wiley-VCH Verlag GmbH, 2006: pp. 315–376. doi:10.1002/9783527616817.ch9.
- [23] J.F. Nagle, S. Tristram-Nagle, Structure of lipid bilayers, *Biochim. Biophys. Acta.* 1469 (2000) 159–195.
- [24] R.J. Lippert, B.D. Lamp, M.D. Porter, Specular Reflection Spectroscopy, in: F. Mirabella (Ed.), *Mod. Tech. Appl. Mol. Spectrosc.*, 1998.

- [25] J. E. Bertie, M. Khalique Ahmed, H. H. Eysel, Infrared intensities of liquids. 5. Optical and dielectric constants, integrated intensities, and dipole moment derivatives of water and water-d₂ at 22.degree.C, *J. Phys. Chem.* 93 (2002) 2210–2218. doi:10.1021/j100343a008.
- [26] E. Palik, *Handbook of Optical Constants of Solids II*, Academic Press, San Diego, 1998.
- [27] J. Lipkowski, Z. Shi, A. Chen, B. Pettinger, C. Bilger, Ionic adsorption at the Au(111) electrode, *Electrochim. Acta.* 43 (1998) 2875–2888. doi:10.1016/S0013-4686(98)00028-0.
- [28] R. A. Dluhy, R. Mendelsohn, H. L. Casal, H. H. Mantsch, Interaction of dipalmitoylphosphatidylcholine and dimyristoylphosphatidylcholine-d₅₄ mixtures with glycoporphin. A Fourier transform infrared investigation, *Biochemistry.* 22 (2002) 1170–1177. doi:10.1021/bi00274a028.
- [29] H.L. Casal, H. Mantsch, Polymorphic phase behaviour of phospholipid membranes studied by infrared spectroscopy, *Biochim. Biophys. Acta - Biomembr.* 779 (1984) 381–401.
- [30] H.H. Mantsch, R.N. McElhaney, Phospholipid phase transitions in model and biological membranes as studied by infrared spectroscopy, *Chem. Phys. Lipids.* 57 (1991) 213–226. doi:10.1016/0009-3084(91)90077-O.
- [31] J. Umemura, T. Kamata, T. Kawai, T. Takenaka, Quantitative evaluation of molecular orientation in thin Langmuir-Blodgett films by FT-IR transmission and reflection-absorption spectroscopy, *J. Phys. Chem.* 94 (1990) 62–67. doi:10.1021/j100364a009.
- [32] I. Burgess, M. Li, S.L. Horswell, G. Szymanski, J. Lipkowski, J. Majewski, S. Satija, Electric Field-Driven Transformations of a Supported Model Biological Membrane - An Electrochemical and Neutron Reflectivity Study, *Biophys. J.* 86 (2004) 1763–1776. doi:10.1016/S0006-3495(04)74244-7.
- [33] M. Nazrul Islam, Y. Ren, T. Kato, Polarization Modulation Infrared Reflection Absorption Spectroscopy of Gibbs Monolayer at the Air/Water Interface, *Langmuir.* 18 (2002) 9422–9428. doi:10.1021/la0205708.

- [34] H. Wang, C. S. Coss, A. Mudalige, R. L. Polt, J. E. Pemberton, A PM-IRRAS Investigation of Monorhamnolipid Orientation at the Air–Water Interface, *Langmuir*. 29 (2013) 4441–4450. doi:10.1021/la3051725.